so that a particular process might be more effective during a particular period of time.

In this respect, the results from the (R–N) KP1-03 transition would be quite interesting. Indeed its age is 5.6 Myr (ref. 1), so that it could eventually provide a link between the results from Crete and those from Kauai. Unfortunately the sediments in the KP1 03 transition zone are weakly magnetized and furthermore a ferrugineous level is present in this zone[1]. Thus, such measurements would be quite difficult to achieve.

We thank Cor Langereis for invaluable field assistance, H. Zijderveld for many helpful discussions, and K. Hoffman for detailed comments and suggestions. The Director General of the Institute of Geological and Mining Research (IGME) in Athens provided the necessary permits. C. Kissel, S. Sen and M. Villeger helped with the sampling. This work was supported by the French CNRS ATP Géologie et Géophysique des Océans.

Received 24 April; accepted 20 July 1984.

1. Langereis, C. G., Zachariasse, W. J. & Zijderveld, J. D. A. *Mar. Micropaleont* **8**, 261–281 (1983–84).
2. Valet, J. P., Laj, C. *Earth planet. Sci. Lett.* **54**, 53–63 (1981).
3. Valet, J. P., Laj, C. & Langereis, C. G. *Nature* **304**, 330–332 (1983).
4. Valet, J. P. & Laj, C. *Nature* **309**, 90–91 (1984).
5. Fuller, M., Williams, I. & Hoffman, K. A. *Rev. Geophys. Space. Phys.* **2**, 179–203 (1979).
6. Vandenberg, J. *Tectonophysics* **98**, 29–41 (1983).
7. Laj, C., Jamet, M., Sorel, D. & Valente, J. P. *Tectonophysics* **86**, 45–67 (1982).
8. King, R. F. *Mon. Not. R. astr. Soc. Geophys. Suppl.* **7**, 115 (1955).
9. Hoffman, K. A. *Nature* **309**, 90 (1984).
10. Mankinien, E. A., Donnely-Nolan, J. M., Gromme, C. S. & Hearn, B. C. Jr. *U.S. geol. Surv. Prof. Pap.* **1141**, 67–82 (1981).
11. Liddicoat, J. C. *Phil. Trans. R. Soc.* **A306**, 121–128 (1982).
12. Dodson, R. *et al. Geophys. J. R. astr. Soc.* 373–412 (1978).
13. Hoffman, K. A. *Earth planet. Sci. Lett.* **44**, 7–17 (1979).
14. Bogue, S. W. & Coe, R. S. *Nature* **295**, 399–401 (1982).

Density of the ocean crust

R. L. Carlson & G. S. Raskin

Department of Geophysics and Geodynamics Research Program, Texas A&M University, College Station, Texas 77843, USA

The density structure and average density of the oceanic crust have implications for various geological and geophysical problems, including interpretations of gravity data, the variation of lithospheric bouyancy in relation to age, and role and fate of the crust in subduction. But no systematic evaluation of oceanic crustal density has been made and estimates range from 2.85 to 3.0 Mg m^{-3} (refs 1–3). We have made an evaluation based on seismic refraction data in combination with drilling results, laboratory studies of seismic properties of oceanic and ophiolitic rocks, and ophiolite lithostratigraphy. Our preferred value for the mean density of the oceanic crust is 2.89 ± 0.04 Mg m^{-3}.

Seismic refraction data provide the most important constraints on the structure and composition of the oceanic crust. (Seismic models and their interpretation in terms of composition are given in refs 4, 5.) Over the past decade or so, simple three-layer velocity-structure models have given way to more detailed multilayer models, and synthetic seismogram modelling has led to more sophisticated 'gradient' models.

Synthetic seismogram models indicate that the upper 2 km of igneous basement (layer 2) is characterized by strong vertical velocity gradients, with P-wave velocities ranging from <4 km s^{-1} at the top to >6 km s^{-1} at the bottom of the interval. Layer 2 may, nevertheless, be subdivided into layers (2a, 2b, 2c), though these regions may not be homogeneous or separated by distinct discontinuities[5,6]. The rapid increase of velocity with depth in layer 2 may be attributed to several factors: (1) velocities in the upper 200–400 m of the section are significantly reduced by large-scale porosity (produced, for example, by collapsed pillows, and lava tubes)[7–9]; (2) there is a systematic decrease of grain-boundary porosity with depth[10–12]; and (3) metamorphic grade increases with depth; greenschist facies mineral assemblages (chlorite, epidote, actinolite, albite) are associated with layer 2c in hole 504B (ref. 9). In contrast to layer 2, velocity gradients in oceanic layer 3 are low (0.0–0.1 S^{-1}). The velocity at the top of the unit is typically 6.7–6.8 km s^{-1}, but the internal structure of layer 3 is apparently variable. In some cases, the gentle gradient extends to the Moho; in others the layer may be subdivided into two (or more) units[4,5,13]. The transition from crustal to mantle velocities generally occurs over an interval of ~1 km.

The oceanic crust can be approximated by a layered sequence, having an average density given by

$$\rho_{avg} = \frac{1}{T}\sum_{i=1}^{n} \rho_i t_i;\ T = \sum_{i=1}^{n} t_i \qquad (1)$$

where ρ_i and t_i are the density and thickness of the ith layer, respectively, n is the total number of layers and T is the total thickness of the sequence. The number of layers and their thicknesses may be taken directly from seismic velocity-structure models; the problem is to find a means of estimating the layer densities. We have approached this problem in three ways.

Some ophiolites, at least, are now believed to be slices of oceanic crust and upper mantle. The velocity structures of the Semail Ophiolite, Oman and the Bay of Islands Complex, Newfoundland, for example, have been reconstructed on the basis of laboratory studies[14–16]. The principal lithologies present in the 'crustal' sections of ophiolites are basalts, diabases, gabbros and their metamorphic equivalents. A much simplified lithologic sequence, viewed from the top downward, consists of extrusive, generally pillowed, basalts (1–1.5 km thick), sheeted diabase dykes (1–1.5 km), and a high-level isotropic gabbro sequence (up to 1 km), which grades downward into a 3–5-km thick sequence of mafic, layered gabbros (hornblende, pyroxene, and olivine gabbro, troctolite, and so on) in which the ultramafic component typically increases with depth. The mafic gabbros are commonly, but not always, interlayered with ultramafic cumulates in the lower part of the 'crustal' section.

The velocity structures of ophiolites are similar to the velocity structure of the oceanic crust[14,15,17]. In ophiolites, 'layer 2' is characterized by strong velocity gradients which extend well into the sheeted dykes and reflect the combined effects of a systematic increase in metamorphic grade (zeolite to upper greenschist facies) and a systematic decrease in grain-boundary porosity with depth[14–17]. Velocities typical of oceanic layer 3 are encountered in the middle to lower part of the dyke sequence, where upper greenschist assemblages give way to those of lower amphibolite grade. The velocity gradient below this level is relatively low, and differences between ophiolites in the amount of modal olivine present in the lower part of the gabbro sequence account for the observed variability of layer 3 velocity structures[16].

In method 1, to estimate crustal density, we assume that layer 2 consists of basalts and dyke rocks in about equal proportions. The upper part of layer 3 is taken to consist of gabbro and metagabbro, with denser, olivine gabbros occurring in the lower half the layer. Neglecting the effect of interlayered ultramafic rocks in the lowermost part of the crustal section, we have used

Table 1 Densities of ophiolite samples

Lithology		No. of samples	Density (Mg m^{-3})
Metabasalt, basalt and spilite	(B)	34	2.73 ± 0.09
Diabase and metadiabase	(D)	31	2.85 ± 0.07
Metagabbro	(MG)	27	2.90 ± 0.07
Gabbro and olivine gabbro	(G + OG)	38	2.95 ± 0.07
Metagabbro, gabbro and olivine gabbro	(G + MG + OG)	65	2.93 ± 0.07

Table 2 Summary of average velocity-structure models and density structures

Model				Method 1		Method 2	Method 3
Ref.	Layer	Thickness (km)	Velocity (km s^{-1})	Lithology*	Density (Mg m^{-3})	Density (Mg m^{-3})	Density (Mg m^{-3})
24	2	1.71 ± 0.75	5.07 ± 0.63	B + D	2.79 ± 0.08	2.63 ± 0.15	2.75 ± 0.09
	3	4.86 ± 1.42	6.69 ± 0.26	G + MG + OG	2.93 ± 0.07	2.91 ± 0.04	2.91 ± 0.04
	Mean				2.89 ± 0.06	2.84 ± 0.06	2.87 ± 0.04
25	2	1.49 ± 0.98	5.19 ± 0.69	B + D	2.79 ± 0.08	2.66 ± 0.16	2.77 ± 0.10
	3	4.62 ± 1.30	6.81 ± 0.16	G + MG + OG	2.93 ± 0.07	2.93 ± 0.03	2.93 ± 0.03
	Mean				2.90 ± 0.06	2.86 ± 0.06	2.89 ± 0.04
4	2	1.39 ± 0.5	5.04 ± 0.69	B + D	2.79 ± 0.08	2.62 ± 0.17	2.75 ± 0.10
	3	4.97 ± 1.25	6.73 ± 0.19	G + MG + OG	2.93 ± 0.07	2.92 ± 0.04	2.92 ± 0.04
	Mean				2.90 ± 0.06	2.85 ± 0.05	2.88 ± 0.04
4	2	1.6	4.4	B + D	2.79 ± 0.08	2.45 ± 0.03‡	2.64 ± 0.01‡
Sonobouy Type I	3a	1.2	6.4	MG	2.90 ± 0.07	2.87 ± 0.03	2.91 ± 0.01
	3b	4.8	7.1	G + OG	2.95 ± 0.07	2.97 ± 0.03	2.97 ± 0.03
	Mean				2.91 ± 0.05	2.84 ± 0.02	2.89 ± 0.02
4	2	1.6	4.4	B + D	2.79 ± 0.08	2.45 ± 0.03	2.64 ± 0.01‡
Sonobouy Type II	3a	3.0	6.8	MG	2.90 ± 0.07	2.93 ± 0.03	2.93 ± 0.03
	3b	2.6	7.5	G + OG	2.95 ± 0.07	3.01 ± 0.01	3.01 ± 0.02
	Mean				2.89 ± 0.04	2.85 ± 0.02	2.89 ± 0.01
6	2a	0.3 ± 0.1	3.74 ± 0.50	B	2.73 ± 0.09	2.21 ± 0.22	2.49 ± 0.14
Atlantic	2b	1.0 ± 0.1	5.13 ± 0.38	B + D	2.79 ± 0.08	2.64 ± 0.09	2.76 ± 0.06
	2c	1.0 ± 0.3	6.05 ± 0.22	D	2.85 ± 0.07	2.82 ± 0.05	2.87 ± 0.03
	3	4.97 ± 1.25†	6.83 ± 0.21	G + MG + OG	2.93 ± 0.07	2.93 ± 0.04	2.93 ± 0.04
	Mean				2.89 ± 0.05	2.85 ± 0.04	2.88 ± 0.03
6	2a	0.4 ± 0.1	3.47 ± 0.35	B	2.73 ± 0.09	2.08 ± 0.18	2.41 ± 0.11
Pacific	2b	0.8 ± 0.1	5.28 ± 0.39	B + D	2.79 ± 0.08	2.68 ± 0.09	2.78 ± 0.05
	2c	0.9 ± 0.4	6.12 ± 0.18	D	2.85 ± 0.07	2.83 ± 0.04	2.88 ± 0.02
	3	4.97 ± 1.25†	6.90 ± 0.17	G + MG + OG	2.93 ± 0.07	2.94 ± 0.03	2.94 ± 0.03
	Mean				2.89 ± 0.05	2.85 ± 0.03	2.89 ± 0.03
13	2a	0.38	5.30	B + D	2.79 ± 0.08	2.68 ± 0.03‡	2.78 ± 0.01‡
	2b	1.93	6.10	D	2.85 ± 0.07	2.83 ± 0.03	2.88 ± 0.01
	3a	1.55	6.86	MG	2.90 ± 0.07	2.94 ± 0.03	2.94 ± 0.03
	3b	3.15	7.06	G + OG	2.95 ± 0.07	2.96 ± 0.03	2.96 ± 0.03
	Mean				2.90 ± 0.04	2.90 ± 0.01	2.92 ± 0.01

* Abbreviations as in Table 1.
† Thickness of layer taken from the average structure of Christensen and Salisbury[4].
‡ Calculated standard deviations do not include the effect of variability in crustal structure.

published water-saturated bulk densities[14–17] to estimate the mean densities of pertinent combinations of rock types given in Table 1.

Assigning densities to velocity structure models on the basis of ophiolite lithostratigraphy neglects the large-scale porosity of layer 2a (refs 7, 8), and is based on a lithologic model which is only loosely tied to the velocity structure. A preferable approach is one in which layer densities can be calculated from a statistically-valid, functional relationship between formation density and seismic velocity.

Assuming that the variation of grain properties is small relative to the difference between the properties of the grains and those of the pore medium (seawater), we may combine the theoretical density and time-average relations for two-component systems, to obtain a velocity/density function

$$\rho = a + b/V_p \quad (2)$$

Fitting this equation to the laboratory densities and P-wave velocities (measured at 100 MPa) of samples recovered by the Deep Sea Drilling Project and from ophiolites[14–21] (Fig. 1) yields

$$\rho(\text{Mg m}^{-3}) = (3.81 \pm 0.02) - (5.99 \pm 0.11)/V_p(\text{km s}^{-1}) \quad (3)$$

with a coefficient of determination (r^2) of 0.86 and an r.m.s. error of 0.07 Mg m^{-3}. Equation (3) describes the velocity/density relation for oceanic rocks very well.

In method 2 layer densities are calculated from seismic velocities according to equation (3). The relation does not account for increasing confining pressure, but the effect of pressure (above 100 MPa) on density and velocity is relatively small. Equation (3) reflects the effects of grain-boundary porosity and metamorphic grade, but also includes effects of alteration[18–19], which is not representative of oceanic basalts. This method also fails to account for large-scale porosity. Thus method 2 may be applied to deeper levels of the crust where porosity is low, but cannot be applied with confidence to oceanic layer 2.

Seismic velocities in porous media depend on the shapes of the voids as well as the properties of the matrix and pore medium. Because the shapes of large-scale voids in layer 2 are unknown, there are likely to be large uncertainties in the any postulated relationship between velocity and density or porosity[5]. We have, therefore, taken the simplest possible approach of calculating the coefficients of equation (2) from the properties of an average, zero-porosity basalt and the properties of seawater (ρ = 1.025 Mg m^{-3}; V_p = 1.5 km s^{-1}). The average bulk-grain densities of oceanic basalts range from 2.9 to 3.0 Mg m^{-3} (refs 7, 10, 12); we estimate the properties of a typical, zero-porosity basalt to be $\rho = 2.03 \pm 0.06$ Mg m^{-3} and $V_p = 6.65 \pm 0.20$ km s^{-1}. The velocity/density relation is then

$$\rho(\text{Mg m}^{-3}) = (3.50 \pm 0.2) - (3.79 \pm 0.1)/V_p(\text{km s}^{-1}) \quad (4)$$

The velocity/density relation for the porous basalt formation (equation (4)) and for the laboratory data (equation (3)) are shown in Fig. 2.

Also shown in Fig. 2 are velocities and densities estimated from downhole logging in igneous basement at a number of

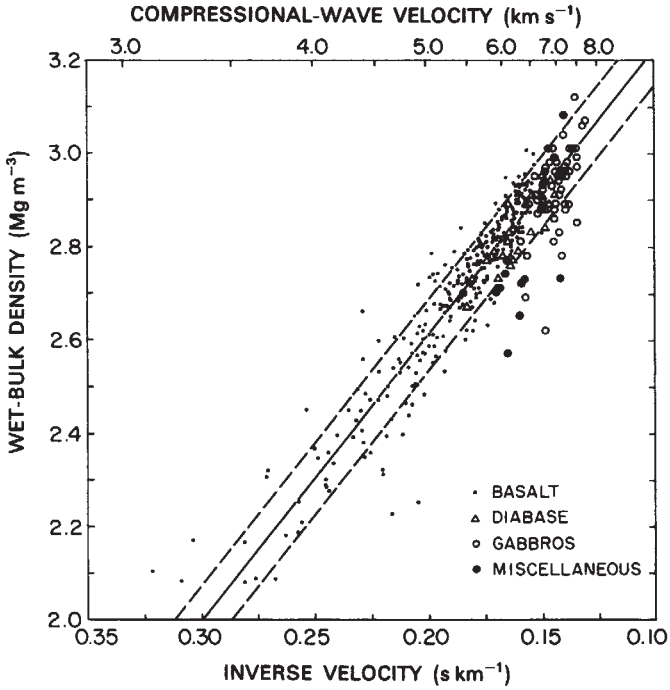

Fig. 1 Compressional-wave velocity versus wet-bulk density of basalts, diabases and gabbroic rocks sampled from ophiolites and recovered from the sea floor by drilling. Also included are some rock types (including serpentinites and amphiliolites) thought to be present but not abundant in the oceanic crust. Solid line represents least-squares fit (equation 3). Dashed lines represent standard error. The r.m.s. misfits to basalt, diabase and gabbro data taken separately range from 0.04 to 0.08 Mg m^{-3}.

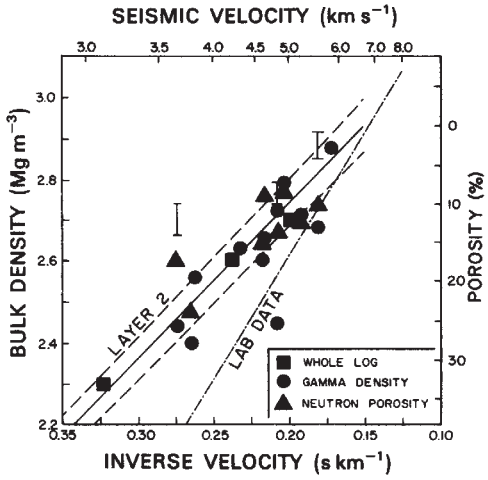

Fig. 2 Approximate velocity–density–porosity relation for a porous basalt formation (layer 2) and best-fitting relation for laboratory data. Also shown are formation velocities, densities and porosities estimated from downhole logs. Bars indicate porosities estimated from wide-spacing resistivity data[23].

DSDP sites. Some of the data are from published reports[8,11,22]. We have made additional, preliminary analyses of logs from holes 504B (Leg 83), 556, 558 and 564. The velocities shown are averages from sonic logs. Gamma–gamma density, neutron porosity and electrical resistivity data[23] have been used to estimate densities and porosities. The neutron porosity values have been corrected for pressure and bound water content as described by Kirkpatrick[8]. Some of the data points represent averages over the entire logged interval; in other cases (such as, Leg 83, 504B) the data points represent different intervals such as layers 2a, 2b and 2c. While we must emphasize that our interpretations of the logs are preliminary, and, therefore, subject to (presumably) minor changes, we find that the data correspond quite well with the predicted relation. The r.m.s. misfits of equation (4) to the log values of density and porosity are 0.06 Mg m^{-3} and 4%, respectively. Insofar is it does agree with available downhole logging data, equation (4) represents a valid means of estimating both the porosity and the density of layer 2 from seismic refraction data.

A particularly important point is that equation (4) predicts markedly higher densities than does the velocity–density relation based on laboratory measurements (equation (3)). For a seismic velocity of 5.0 km s^{-1}, the difference is ~0.15 Mg m^{-3}, for a velocity typical of layer 2a, about 3.75 km s^{-1}, the difference is 0.3 Mg m^{-3}. Thus the common practice of using laboratory data to estimate formation densities from seismic velocities may lead to serious errors when the porosity of the layer is greater than the grain-boundary porosity of the rocks.

In method 3, we have accounted for large-scale porosity of layer 2a by calculating layer densities according to equation (4) when the seismic velocity is <6.65 km s^{-1}. Thus, in general, equation (4) applies to oceanic layer 2. For velocities >6.65 km s^{-1} (layer 3), we have used equation (3).

Any of the three methods outlined above can be applied to an individual refraction survey. Because our objective is to estimate the average density of the oceanic crust, we have used several average velocity structures: three 'standard' three-layer models[4,24,25]; the type I and II sonobouy models of Christensen and Salisbury[4], in which layer 3 is subdivided into two units (3a and 3b); the Atlantic and Pacific multilayer models proposed by Houtz and Ewing[6]; and a four-layer model suggested by Purdy[13] for crust 140 Myr old. The velocity structures, estimated layer densities and mean crustal densities are summarized in Table 2.

A remarkable feature of the results is that the different velocity-structure models yield such similar mean crustal densities: the range of values found by method 1 is 2.89–2.91 Mg m^{-3}, the range for method 2 is, in general, 2.84–2.86 Mg m^{-3}, and most of the densities calculated by method 3 are in the range 2.88–2.90 Mg m^{-3}. Mean crustal densities estimated by methods 1 and 3 are also remarkably similar; the average difference is <0.01 Mg m^{-3}. Method 2 yields mean densities which are systematically lower by ~0.03 Mg m^{-3}. Having calculated the density structures by these methods, the problem is to select the best model.

Method 3 is preferable to the other methods because densities are calculated from the seismic structure, and the large-scale porosity of layer 2 is taken into account. Equation (4) used to estimate the density of layer 2 is also in good general agreement with the results of downhole logging in igneous basement (Fig. 2). Furthermore, the density structures calculated by this method are consistent with the inferred variation of physical properties with depth in the oceanic crust.

Large-scale porosity is generally restricted to the uppermost 400 m (layer 2a) of the section. Below that depth, the porosity is markedly reduced (layer 2b), and below 1,000 m (layers 2c and 3) porosity is apparently restricted to the grain boundaries[6,11,13,23]. Consequently, calculated layer densities (Table 2) should correspond to the densities of corresponding lithologies. Calculated layer 3 densities agree with the mean density of oceanic gabbros (2.93 ± 0.07 Mg m^{-3}). The density of the lower part of layer 2 (2.88) is higher than the mean (2.85 Mg m^{-3}), but agrees with the modal value (2.88 Mg m^{-3}) for diabases. The mean densities of different suites of oceanic basalts range from 2.79 to 2.80 Mg m^{-3} (refs 7, 10, 12). The range of calculated layer 2 mean densities (not included in Table 2) is 2.80–2.75 Mg m^{-3}. These values range downward from the mean for basalts and diabases because of the porosity of layer 2a, but the effect of porosity on the average density of layer 2 is reduced because the porous region occupies only ~20% of the layer thickness.

Thus, we conclude that density structures calculated by method 3 are representative of *in situ* densities in the oceanic

crust. A reasonable mean density is 2.89 ± 0.04 Mg m^{-3}. Even if we assume that 500 m of ultramafic cumulates having a density of 3.20 Mg m^{-3} should be included, the mean crustal density is only 2.91 Mg m^{-3}. The proposed existence of a low-velocity layer of partially serpentinized periodotites at the base of the crust[26] would not significantly affect its density because the density of periodotites containing 50% serpentine is ~2.9 Mg m^{-3} (ref. 27). Including a 500-m blanket of sediments having a mean density of 2.0 Mg m^{-3} reduces the density of the entire crust to ~2.85 Mg m^{-3}.

This research was supported by Office of Naval Research Contract N-00014-80-C-0013. N. L. Carter's suggestions substantially improved the manuscript. Texas A&M Geodynamics Research Program contribution no. 44.

Received 11 May; accepted 31 July 1984.

1. Watts, A. B. *J. geophys. Res.* **83**, 5989–6004 (1978).
2. Molnar, P. & Atwater, T. *Earth planet. Sci. Lett.* **41**, 330–340 (1978).
3. Pennington, W. D. *Tectonophysics* **102**, 377–398 (1984).
4. Christensen, N. I. & Salisbury, M. H. *Rev. Geophys. Space Phys.* **13**, 57–86 (1975).
5. Spudich, P. & Orcutt, J. *Rev. Geophys. Space Phys.* **18**, 627–645 (1980).
6. Houtz, R. & Ewing, J. *J. geophys. Res.* **81**, 2490–2498 (1976).
7. Hyndman, R. D. & Drury, M. J. *J. geophys. Res.* **81**, 4042–4052 (1976).
8. Kirkpatrick, R. J. *J. geophys. Res.* **84**, 178–188 (1979).
9. Anderson, R. N. *et al. Nature* **300**, 589–594 (1982).
10. Hamano, Y. *Init. Rep. DSDP Legs* **51, 53** Part 2, 1457–1466 (1980).
11. Salisbury, M. H. *et al. Init. Rep. DSDP Legs* **51, 53** Part 2, 1579–1597 (1980).
12. Karato *et al. Init. Rep. DSDP Leg* **69**, 675–682 (1981).
13. Purdy, G. M. *Geophys. J. R. astr. Soc.* **72**, 115–137 (1983).
14. Salisbury, M. H. & Christensen, N. I. *J. geophys. Res.* **83**, 805–817 (1978).
15. Christensen, N. I. & Smewing, J. D. *J. geophys. Res.* **86**, 2545–2556 (1981).
16. Christensen, N. I. & Salisbury, M. H. *Geophys. J. R. astr. Soc.* **68**, 675–688 (1982).
17. Christensen, N. I. *Tectonophysics* **47**, 131–157 (1978).
18. Christensen, N. I. & Salisbury, M. H. *Earth planet. Sci. Lett.* **15**, 367–375 (1972).
19. Christensen, N. I. & Salisbury, M. H. *Earth planet. Sci. Lett.* **19**, 461–470 (1973).
20. Fountain, D. M. *et al. Mar. Geol.* **19**, M75–M80 (1975).
21. Carlson, R. L. & Wilkens, R. H. *Geodyn. Ser.* **11**, 127–136 (1983).
22. Cann, J. R. & Von Herzon, R. P. *Init. Rep. DSDP Leg* **69**, 281–299 (1981).
23. Becker, K. *et al. Nature* **300**, 594–598 (1982).
24. Raitt, R. in *The Sea* Vol. 3 (ed. Hill, M. N.) 85–102 (Wiley, New York, 1963).
25. Shor, G. G. in *The Sea* Vol. 7 (ed. Maxwell, A.) 3–27 (Wiley, New York, 1971).
26. Lewis, B. T. R. & Snydsman, W. *Nature* **266**, 340–344 (1977).
27. Carlson, R. L. *et al. Earth planet. Sci. Lett.* **51**, 171–180 (1980).

Growing season precipitation from D/H ratios of Eastern White Pine

J. R. Lawrence* & J. W. C. White

Lamont-Doherty Geological Observatory of Columbia University, Palisades, New York 10964, USA

The search for climatic information from the hydrogen and oxygen isotope analysis of tree rings has produced mixed results[1–6]. Systematic changes in the D/H ratio with changing climate have been demonstrated[7], although relationships between climate change and the D/H ratio in tree rings from a single tree have been claimed, the interpretation of these data still causes controversy. Here we report that there is a strong correlation between both the D/H ratio of summer rain and tree ring cellulose from Eastern White Pine (*Pinus strobus* L.), and the amount of precipitation between May and August.

There are three major difficulties in interpreting the isotope composition of tree ring cellulose. (1) Organic matter is isotopically inhomogeneous[4,7–11]. (2) Complex biological, biochemical and hydrological processes take place during the growth of a tree[7,12–15]. (3) Isotope variations in precipitation from year to year at a single location have not been clearly related to temperature changes, except perhaps for those that accompany significant changes in the polar ice caps[16–18]. We have avoided the problem of the isotopic inhomogeneity of organic matter by analysing only carbon-bound hydrogen from cellulose[7]. Our studies of the complex isotopic fractionations resulting from biological, biochemical and hydrological processes in Eastern White Pine are reported elsewhere[19,20]. They demonstrate that the average hydrogen isotope composition of rain that falls during the growing season, May–August, can be found in tree rings of Eastern White Pine growing under highly restricted water supply conditions. Such trees mostly use soil moisture obtained from summer precipitation and therefore retain only a summer climate signal.

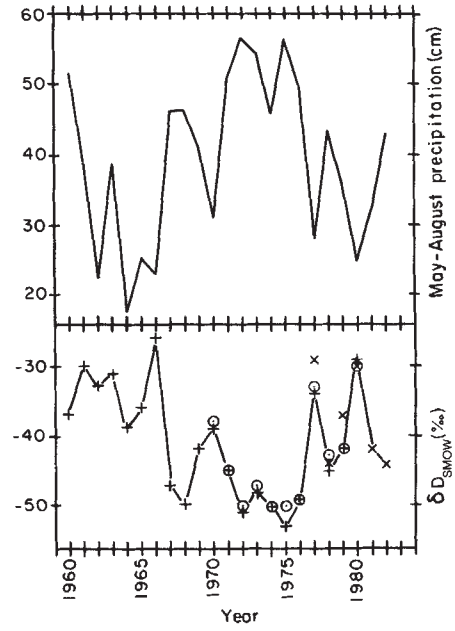

Fig. 1 Average amount of precipitation for the period May–August for five meteorological stations (Mohonk Lake, Poughkeepsie, Ellenville, Gardiner and Rosendale) plotted as a function of time. The δD values of rain and carbon-bound hydrogen from tree rings of two Eastern White Pine trees are also plotted. One tree covers the period 1960–80 (+), the other the period 1970–80 (○) and the rain from 1977–82 (×). The correlation coefficients between the δD values and the amount of May to August precipitation are −0.76, −0.93 and −0.88 respectively.

One climate signal that has been observed from stable isotopes in the precipitation from lower latitudes, is the inverse relationship between the δD and δ^{18}O of rain and the amount of precipitation. ($\delta D = [(D/H \text{ sample})/(D/H \text{ SMOW} - 1)] \times 10^3$, where SMOW is standard mean ocean water.) This 'amount effect' was observed by Dansgaard[21] when evaluating monthly precipitation samples obtained and analysed by the International Atomic Energy Agency (IAEA). He observed that isotopic ratios were "low in rainy months and high in months with sparse rain". He stated: "this 'amount effect' is found all the year round at most tropical stations, and in the summer time at mid latitudes", this rain being predominantly produced by convective storms. We also detected this amount effect during the present investigation.

Our sampling location, Mohonk Lake, New York, is located ~130 km north of New York City on the Schawangunk ridge on the west side of the Hudson Valley near New Paltz, New York. The two Eastern White Pine trees studied are located on a talus slope where groundwater has not been detected in the tree sap[20]. The trees are ~5 m high, 60 cm in diameter and >200-yr old.

The δD values of the rings from these trees together with the unweighted average δD value of all the individual rainfalls between May and August are plotted as a function of time in Fig. 1. One tree (no. 1) covers the period 1960–80, the other tree (no. 2) 1970–80 and the rains from 1977 to 1982. Also shown in Fig. 1 is the total amount of rain that fell between May and August of each year. These quantities represent the averages of five rain recording stations in the vicinity of Mohonk Lake.

An inverse relationship can be seen between the amount of precipitation and the isotope data (Fig. 1): years of high precipi-

* Present address: Department of Geological Sciences, University of Houston, Texas 77004, USA.